Size-dependent piezoelectricity: A 2D finite element formulation for electric field-mean curvature coupling in dielectrics

Bradley T. Darrall, Ali R. Hadjesfandiari, Gary F. Dargush*
Department of Mechanical and Aerospace Engineering
University at Buffalo, State University of New York
Buffalo, NY 14226 USA

ABSTRACT

The classical theory of piezoelectricity defines linear size-independent electromechanical response in non-centrosymmetric dielectrics that involves coupling between the electric field and the mechanical strains. However, with the continuing push to develop novel micro- and nano-scale materials, structures and devices, there is a need to refine and explore size-dependent electro-mechanical coupling phenomena, which have been observed in experiments on centrosymmetric dielectrics. Here a finite element variational formulation is developed based upon a recent consistent size-dependent theory that incorporates the interactions between the electric field and the mechanical mean curvatures in dielectrics, including those with centrosymmetric structure. The underlying formulation is theoretically consistent in several important aspects. In particular, the electric field equations are consistent with Maxwell's equations, while the mechanical field equations are based upon the recent consistent couple stress theory, involving skew-symmetric mean curvature and couple stress tensors. This, in turn, permits the development of a fully-consistent finite element method for the solution of size-dependent piezoelectric boundary value problems. In this paper, an overview of size-dependent piezoelectricity is first provided, followed by the development of the variational formulation and finite element representation specialized for the planar response of centrosymmetric cubic and isotropic materials. The new formulation is then applied to several illustrative examples to bring out important characteristics predicted by this consistent size-dependent piezoelectric theory.

Keywords: Flexoelectricity; Size-dependent mechanics; Couple stresses; Multiphysics problems; Mixed finite element methods

* Corresponding author. Tel.: +1 716 645 2315; fax: +1 716 645 2883.
E-mail addresses: bdarrall@buffalo.edu (B.T. Darrall), ah@buffalo.edu (A.R. Hadjesfandiari), gdargush@ buffalo.edu (G.F. Dargush).

1. Introduction

Over the last half-century, piezoelectric phenomena have had a profound impact on the development of many technologies. More recently, however, there is a push to develop technology on increasingly minute length scales, where it has been discovered that classical piezoelectric theory is not sufficient for describing all of the observed linear electromechanical coupling behavior. For modeling of small-scale electromechanical phenomena, a size-dependent piezoelectric theory, in some forms known as flexoelectricity, is necessary. These proposed theories are higher order continuum theories that include coupling between a higher order measure of deformation, such as strain-gradient or curvature, and the electric polarization field. Interestingly, it is shown both experimentally and theoretically that these size-dependent piezoelectric effects can occur in classically non-piezoelectric materials and, in particular, centrosymmetric cubic and isotropic materials.

Classical piezoelectricity describes the linear electromechanical coupling between strain or stress and the polarization within an anisotropic dielectric body. The groundbreaking experimental work of the Curie brothers established the foundation for piezoelectricity (Curie and Curie, 1880), which was subsequently placed on a firm theoretical base by Voigt (1910). The well-known monograph by Cady (1964) provides a comprehensive review of developments through the middle of the twentieth century. Since then countless technologies have taken advantage of piezoelectric phenomenon, from high-tech instrumentation to everyday commercial products.

The idea of size-dependent piezoelectric effects was first discussed in Kogan (1964), Meyer (1969) and Tagantsev (1986) and was eventually coined "flexoelectric" effects. More recently size-dependent piezoelectric effects and electromechanical coupling effects in centrosymmetric bodies have been studied by numerous researchers (e.g., Mishima et al., 1997; Shvartsman et al., 2002; Buhlmann et al., 2002; Cross, 2006; Maranganti et al., 2006; Harden et al., 2006; Zhu et al., 2006; Sharma et al., 2007; Majdoub et al., 2008; Maranganti and Sharma, 2009; Resta, 2010; Baskaran et al., 2011; Catalan et al., 2011). With the increasing development of micro- and nano-scale technology, there is a need to model this size-dependent piezoelectric behavior, which can have useful effects for small characteristic geometries and cannot be captured using classical piezoelectric theory. This size-dependent behavior can be incorporated by considering that besides strain, the polarization in a dielectric body may be coupled to higher order measures of deformation as well. It is logical when formulating a size-dependent piezoelectric theory to consider a size-dependent elasticity theory and then introduce electromechanical coupling via thermodynamic considerations. Wang et al. (2004) consider the gradient of rotation as the higher order measure of deformation, which then is coupled to the polarization. Others have considered strain gradients and various forms of curvature to be coupled to the electric polarization (Tagantsev, 1986; Sharma et al., 2007; Eliseev et al. (2009). The previous theories suffer either from various incompatibility with the underlying Maxwell equations of electromagnetics

(Hadjesfandiari, 2014) or with inherent indeterminacies due to the dependence on original couple-stress elasticity theories, as first developed by Toupin (1962), Mindlin and Tiersten (1962) and Koiter (1964).

Recently, the consistent couple-stress theory was developed, which remedied the issues that prior size-dependent elasticity theories had (Hadjesfandiari and Dargush, 2011, 2013). In this new theory, the mean curvature tensor is shown to be the correct higher order measure of deformation, while the skew-symmetric nature of the couple-stress tensor is revealed, making the theory fully determinate. More recently, in Hadjesfandiari (2013), a new consistent size-dependent piezoelectric theory is advanced by using the discoveries in Hadjesfandiari and Dargush (2011, 2013) regarding size-dependent elasticity. This new theory has coupling between the skew-symmetric mean curvature tensor and the polarization field, which allows for piezoelectric behavior even in centrosymmetric materials. Couple-stress effects are also inherently present in this theory (Hadjesfandiari, 2013).

In order for technology to take full advantage of piezoelectric phenomena, numerical methods for accurate modeling must be developed. Similar to most continuum theories, the only available analytical solutions for piezoelectric problems are based on very simple geometry and boundary conditions. To date, many finite element based formulations have been developed for modeling classical piezoelectricity. Benjeddou (2000) gives an excellent review of the advances in finite element approaches to modeling piezoelectric structural elements. Other notable works on finite element formulations for classical piezoelectricity include those of Allik and Hughes (1970) for applications to vibration, Hwang et al. (1993) for modeling of sensors and actuators, and Gaudenzi and Bathe (1995) for general continua analysis.

Despite the many efforts to advance numerical methods used to model and simulate classical piezoelectricity, very little work has been done in developing numerical methods to model size-dependent piezoelectric effects. Consequently, in this paper, we develop a mixed finite element (FE) formulation that can be applied to solve planar size-dependent piezoelectric problems. Because much work has already been done to develop finite element formulations for classical piezoelectric effects that can only exist in non-centrosymmetric anisotropic materials, we instead restrict ourselves to centrosymmetric materials. Most interestingly, higher order size-dependent piezoelectric effects can still be present for such materials, which in turn suggest many potential new applications at the micro- and nano-scale.

The formulation presented here is based on the consistent size-dependent piezoelectric theory of Hadjesfandiari (2013), while the finite element formulation can be considered an extension of the consistent couple-stress variational finite element approach developed by the present authors (Darrall et al., 2014). This new size-dependent piezoelectric FE formulation is based on the variational problem that is derived from considering the stationarity of a total electromechanical

enthalpy functional. The electric field is coupled to the mean curvature within the electromechanical enthalpy, which allows for size-dependent piezoelectric effects. By considering the rotation to be an additional field variable and then enforcing rotation-displacement compatibility via Lagrange multipliers, the coupled size-dependent piezoelectricity problem is reduced to a C^0 variational problem. This type of formulation is made more attractive by the fact that these Lagrange multipliers are shown in Darrall et al. (2014) to be equal to the skew-symmetric portion of the stress tensor, which otherwise would be difficult to obtain in an efficient and accurate manner.

Throughout this paper, standard tensor index notation will be used where subscripts i, j, k, and l will range from 1 to 3 representing Cartesian coordinates x, y, and z. Repeating of indices implies summing over all values for that index. Additionally, ε_{ijk} is the Levi-Civita alternating symbol and δ_{ij} is the Kronecker delta. In Section 3, vector notation is used for convenience, where bold face characters will be used to represent vectors and matrices.

The remainder of the paper is organized as follows. Section 2 provides an overview of size-dependent piezoelectric theory for centrosymmetric materials and introduces the mixed variational principle upon which the finite element formulation is based. In Section 3, the corresponding finite element formulation is developed in detail. Then, in Section 4, we employ this new FE formulation to analyze four problems. First, the formulation is validated by comparing to the analytical solution of a long cylinder in a uniform electric field. The second problem analyzed is a cantilever subject to constant transverse electric field, which has significance to sensors and actuators. Results are compared to the beam model developed in Li et al. (2014). This same problem setting is then carried out for a cantilever consisting of Barium Titanate in the following subsection. These three problems all involve the converse size-dependent piezoelectric effect, in which an electric field induces a mechanical response. The final problem illustrates the direct size-dependent piezoelectric effect in isotropic media, having an electric field induced by an applied mechanical load. Finally, a number of conclusions are presented in Section 5.

2. Linear size-dependent piezoelectricity in a centrosymmetric material

In this section, a brief overview of the important concepts and relations of consistent size-dependent piezoelectricity theory is provided, based entirely on the work of Hadjesfandiari (2013). Particular attention is given to relations pertinent to the development of the finite element formulation presented in the next section. For a more detailed discussion on consistent size-dependent piezoelectricity, the reader is referred to Hadjesfandiari (2013).

At its simplest, linear size-dependent piezoelectricity can be described as the linear thermodynamic coupling between size-dependent elasticity and the electric polarization of a material. The theory presented here is based on the consistent skew-symmetric couple-stress theory (Hadjesfandiari and Dargush, 2011, 2013), which sets it apart from other size-dependent piezoelectricity and flexoelectricity theories. Furthermore, unlike the commonly accepted flexoelectric theory, the present formulation is consistent with Maxwell's equations of electromagnetism, which would seem to be a most important requirement. Details on the comparison can be found in Hadjesfandiari (2014). Because the present work is on size-dependent piezoelectricity as defined by Hadjesfandiari (2013), primary focus will be given to the extension of skew-symmetric couple-stress theory and not the fundamentals of the purely mechanical theory. For a detailed description of skew-symmetric couple-stress theory, the reader is referred to Hadjesfandiari and Dargush (2011, 2013).

From couple-stress theory, a general three dimensional body under quasistatic conditions is governed throughout its volume V by the following equilibrium equations coming from linear and angular momentum balance, respectively,

$$\sigma_{ji,j} + \bar{F}_i = 0 \tag{1}$$
$$\mu_{ji,j} + \varepsilon_{ijk}\sigma_{jk} = 0 \tag{2}$$

where σ_{ji} and μ_{ji} are the force-stresses and couple-stresses, respectively, while $\bar{F}_i$ represents applied body force densities. The consideration of body couples is shown to be redundant in Hadjesfandiari and Dargush (2011).

In addition, the body is subject to boundary conditions on the surface S. Let us assume that the natural boundary conditions take the form

$$t_i = \bar{t}_i \quad \text{on} \quad S_t \tag{3a}$$
$$m_i = \bar{m}_i \quad \text{on} \quad S_m \tag{3b}$$

while the essential boundary conditions can be written

$$u_i = \bar{u}_i \quad \text{on} \quad S_u \tag{4a}$$
$$\omega_i = \bar{\omega}_i \quad \text{on} \quad S_\omega \tag{4b}$$

Here t_i and m_i represent the force-tractions and moment-tractions, respectively, while u_i and ω_i are the displacements and rotations, respectively, and the overbars denote the specified values. For a well-defined boundary value problem, we should have $S_t \cup S_u = S$, $S_t \cap S_u = \emptyset$ and $S_m \cup S_\omega = S$, $S_m \cap S_\omega = \emptyset$. Clearly, more complicated boundary conditions could be specified, but the simplest forms defined in (3) and (4) suffice for the present work.

In general, the relations between force-stress and force-traction, and couple-stress and moment-traction can be written

$$t_i = \sigma_{ji} n_j \tag{5a}$$

$$m_i = \mu_{ji} n_j \tag{5b}$$

where n_i represents the outward unit normal vector to the surface S.

Taking the gradient of the displacement field and splitting it into its symmetric and skew-symmetric parts

$$u_{(i,j)} = e_{ij} = \frac{1}{2}(u_{i,j} + u_{j,i}) \tag{6a}$$

$$u_{[i,j]} = \omega_{ij} = \frac{1}{2}(u_{i,j} - u_{j,i}) \tag{6b}$$

where the parentheses around the indices denote the symmetric part of the tensor and the square brackets represent the skew-symmetric part of the tensor. Here e_{ij} is the linear strain tensor and ω_{ij} is the rotation tensor. Because ω_{ij} is a skew-symmetric tensor with three independent values, it can be represented by a pseudo-vector. According to the right hand convention, the rotation vector is defined as follows

$$\omega_i = \frac{1}{2}\varepsilon_{ijk}\omega_{kj} \tag{7}$$

Then, the relationship between displacement and rotation can be expressed as

$$\omega_i = \frac{1}{2}\varepsilon_{ijk}u_{k,j} \tag{8}$$

By taking the gradient of the rotation field and only considering the skew-symmetric contribution, we are left with the mean curvature tensor

$$\kappa_{ij} = \omega_{[i,j]} = \frac{1}{2}(\omega_{i,j} - \omega_{j.i}) \tag{9}$$

Because the mean curvature tensor is skew-symmetric, it also can be represented in vector form through the following relation

$$\kappa_i = \frac{1}{2}\varepsilon_{ijk}\kappa_{kj} \tag{10}$$

However, in Darrall et al. (2014), we have shown that the more convenient curvature vector is instead the engineering mean curvature vector defined as

$$k_i = -2\kappa_i = \varepsilon_{ijk}\kappa_{jk} \tag{11}$$

Here we have that the "concave upwards" curvature of orthogonal planes is positive and we do not need to include a factor of one-half. The components of k_i are then consistent with the usual mathematical definition of mean curvatures of the three orthogonal planes oriented with the global axes at a point. Furthermore, use of k_i, as opposed to the mean curvature κ_i, alleviates the need to introduce factors of minus two into the energy conjugacy relations.

In Hadjesfandiari and Dargush (2011, 2013), the skew-symmetric nature of the couple-stress tensor is shown through different but equally valid arguments. Because the couple-stress tensor is skew-symmetric, it also may be represented by a corresponding vector, μ_i, where

$$\mu_i = \tfrac{1}{2}\varepsilon_{ijk}\mu_{kj} \tag{12}$$

For a consistent size-dependent elasticity theory, it is shown that mean curvature is the correct energy conjugate quantity to the couple-stress tensor. Alternatively, the engineering curvature vector is the correct energy conjugate quantity to the couple-stress vector.

The couple-stress is related to the skew-symmetric portion of the stress tensor by

$$\sigma_{[ji]} = -\mu_{[i,j]} = -\tfrac{1}{2}\left(\mu_{i,j} - \mu_{j,i}\right) \tag{13}$$

Naturally, this skew-symmetric portion can be represented as a pseudo vector s_i as well, such that

$$s_i = \tfrac{1}{2}\varepsilon_{ijk}\sigma_{[kj]} \tag{14}$$

and

$$\varepsilon_{ijk}s_k = \sigma_{[ji]} \tag{15}$$

For a quasistatic electric field, E_i, we know that the curl vanishes. Because of this, we can relate the electric field to the gradient of a scalar electric potential φ, such that (Griffiths, 1989)

$$E_i = -\varphi_{,i} \tag{16}$$

In a piezoelectric material, an internal polarization field can be induced by deformation and the electric field. It is often convenient, however, to consider the electric displacement field, which is related to the electric field and polarization by

$$D_i = \varepsilon_o E_i + P_i \tag{17}$$

where D_i is the electric displacement vector and P_i is the polarization. For linear dielectric materials, the polarization can be related to the electric field in a linear fashion, and hence so can the electric displacement.

The normal component of the electric displacement, $\mathcal{d}$, on the surface is related to D_i by

$$\mathcal{d} = D_i n_i \tag{18}$$

The governing differential equation for the electric displacement in a dielectric body is the Gauss law in differential form, given by

$$D_{i,i} = \bar{\rho}_E \tag{19}$$

where $\bar{\rho}_E$ is an applied body charge density. Note that this is a scalar quantity and the subscript is merely meant to distinguish the body charge density from the mass density.

At the interface between two different materials, the normal electric displacement is related to the free surface charge, q_s, by

$$q_s = \lfloor \mathcal{d} \rfloor \tag{20}$$

where $\lfloor \cdot \rfloor$ denotes the jump across the interface. It is common in other works to specify free surface charge for the natural boundary conditions related to the electric displacement. However, this is only valid when the external electric displacement is negligible. More generally, the natural boundary conditions can be specified in terms of $\mathcal{d}$, which is what will be used here. Then, for natural and essential boundary conditions, respectively, we have the following:

$$\mathcal{d} = \bar{\mathcal{d}} \quad \text{on} \quad S_{\mathcal{d}} \tag{21}$$

and

$$\varphi = \bar{\varphi} \quad \text{on} \quad S_{\varphi} \tag{22}$$

For a well-defined boundary value problem, we should have $S_{\mathcal{d}} \cup S_{\varphi} = S$, and $S_{\mathcal{d}} \cap S_{\varphi} = \emptyset$.

From Hadjesfandiari (2013), the electromechanical enthalpy density, H, of a linear, centrosymmetric material can be expressed as

$$H = \frac{1}{2} e_{ij} c_{ijkl} e_{kl} + \frac{1}{2} k_i b_{ij} k_j - \frac{1}{2} E_i \varepsilon_{ij} E_j - E_i \gamma_{ij} k_j \tag{23}$$

where c_{ijkl} is the standard 4th order constitutive tensor used for classical linear elasticity theories. In the isotropic case, the response depends on two elastic coefficients, for example, the Lamé constants λ and G. For cubic materials with centrosymmetry, there are three independent elastic coefficients c_{1111}, c_{1122} and c_{1212}, which in Voigt notation are written instead as c_{11}, c_{12} and c_{44}, respectively. More detail can be found in Hadjesfandiari (2014).

In addition, b_{ij} is the 2nd order linear couple-stress-curvature constitutive tensor, ε_{ij} is the total electric permittivity tensor and γ_{ij} is the coupling tensor for the electric field and curvature. The presence of this coupling term in the electric enthalpy is what allows for piezoelectric effects within a centrosymmetric body. For isotropic and centrosymmetric cubic materials, this

piezoelectric-curvature coupling tensor can be written in terms of a single piezoelectric-curvature parameter, $\check{f}$, as

$$\gamma_{ij} = 2\,\check{f}\,\delta_{ij} \tag{24}$$

The piezoelectric-curvature parameter used in this paper is related to the parameter, f, defined in Hadjesfandiari (2013), such that

$$\check{f} = -f \tag{25}$$

This sign change of $\check{f}$ relative to f is a consequence of the choice of curvature vector that is used in the present paper. By using this definition of the piezoelectric-curvature parameter, we have that for materials with positive $\check{f}$, an electric field directed in the positive direction will induce positive ("concave upwards") curvature deformation and vice versa. The electric enthalpy density of course remains unchanged by this choice of parameter.

The total electric permittivity tensor is

$$\varepsilon_{ij} = \varepsilon_r \varepsilon_0 \delta_{ij} \tag{26}$$

while the couple-stress constitutive tensor for centrosymmetric cubic and isotropic materials is

$$b_{ij} = 4\eta\delta_{ij} \tag{27}$$

where ε_0 is the electric permittivity in a vacuum, ε_r is the relative electric permittivity, and η is the couple-stress parameter.

Interestingly, the ratio of the couple-stress parameter to the shear modulus results in a characteristic material length, l, where we have

$$\frac{\eta}{G} = l^2 \tag{28a}$$

for the isotropic case (Hadjesfandiari and Dargush, 2011), while

$$\frac{\eta}{c_{44}} = l^2 \tag{28b}$$

in cubic crystals with centrosymmetry. It is expected that couple-stress effects, and by extension size-dependent piezoelectric effects, are only relevant for length scales comparable to l.

More generally, H could also include coupling between strain and curvature, and of course strain and electric field, such as for classical piezoelectricity, however these coupled effects do not exist in the centrosymmetric dielectric materials we are considering here. Also, it is equally valid to write H in terms of the mean curvature tensor; however from now on in this paper we will use the engineering mean curvature vector for simplicity.

The electromechanical enthalpy density is related to the positive definite internal energy density, U, by

$$H = U - E_i D_i \tag{29}$$

Hadjesfandiari (2013) derives the constitutive equations for the symmetric stress, electric displacement, and couple-stress from H as follows:

$$\sigma_{(ji)} = \frac{\partial H}{\partial e_{ij}} = c_{ijkl} e_{kl} \tag{30a}$$

$$\mu_i = \frac{\partial H}{\partial k_i} = b_{ij} k_j - \gamma_{ji} E_j \tag{31a}$$

$$D_i = -\frac{\partial H}{\partial E_i} = \varepsilon_{ij} E_j + \gamma_{ij} k_j \tag{32a}$$

For an isotropic material, these reduce to (Hadjesfandiari, 2013)

$$\sigma_{(ji)} = \lambda e_{kk} \delta_{ij} + 2G e_{ij} \tag{30b}$$

$$\mu_i = 4G l^2 k_i - 2\check{f} E_i \tag{31b}$$

$$D_i = \varepsilon E_i + 2\check{f} k_i \tag{32b}$$

while for centrosymmetric cubic material, the corresponding relations are given in Hadjesfandiari (2014).

The total electromechanical enthalpy of the system Π_H is defined in Hadjesfandiari (2013) as

$$\Pi_H = \int_V H \, dV + \mathcal{W} \tag{33}$$

where $\mathcal{W}$ is the total potential from applied forces, moments, and normal electric displacement given by

$$\mathcal{W} = -\int_V u_i \bar{F}_i \, dV + \int_V \varphi \bar{\rho}_E \, dV - \int_{S_t} u_i \bar{t}_i \, dS - \int_{S_m} \omega_i \bar{m}_i \, dS - \int_{S_d} \varphi \bar{d} \, dS \tag{34}$$

Therefore, for the total electromechanical enthalpy Π_H, we have

$$\begin{aligned} \Pi_H = {} & \frac{1}{2}\int_V e_{ij} c_{ijlm} e_{lm} \, dV + \frac{1}{2}\int_V k_i b_{ij} k_j \, dV - \frac{1}{2}\int_V E_i \varepsilon_{ij} E_j \, dV - \int_V E_i \gamma_{ij} k_j \, dV - \int_V u_i \bar{F}_i \, dV \\ & + \int_V \varphi \bar{\rho}_E \, dV - \int_{S_t} u_i \bar{t}_i \, dS - \int_{S_m} \omega_i \bar{m}_i \, dS - \int_{S_d} \varphi \bar{d} \, dS \end{aligned} \tag{35}$$

By substituting the kinematic relations, this total electromechanical enthalpy can of course be written as a function of only displacement and electric potential

$$\Pi_H \equiv \Pi_H(e(u), k(u), u, E(\varphi)\,) \tag{36}$$

Now this functional may be extremized by taking the first variation and setting it equal to zero. This however leads to a formulation that requires C^1 continuity of the displacement field.

A better approach, as shown for the purely mechanical problem in Darrall et al. (2014), is to consider independent displacements and rotations and then enforce the rotation-displacement compatibility constraint of (8) by including Lagrange multipliers into the enthalpy functional prior to extremizing. Thus, we define a new functional

$$\Pi_H^* \equiv \Pi_H^*(\, e(u), k(\omega), u, \omega, E(\varphi), \lambda) \tag{37}$$

where

$$\Pi_H^* = \Pi_H + \int_V \lambda_k\big(\varepsilon_{kji} u_{i,j} - 2\omega_k\big) dV \tag{38}$$

It is shown in Darrall et al. (2014) by extremizing the functional for the mechanical problem that these Lagrange multipliers turn out to be equal to the skew-symmetric stress vector, s_i. This is an extremely convenient property of the variational formulation, because otherwise the skew-symmetric part of the stress tensor would be difficult to obtain. The same feature carries over to the couple stress piezoelectric variational principle presented here.

We then have the following C^0 variational problem

$$\delta\Pi_H^* = \frac{\partial \Pi_H^*}{\partial u_i}\delta u_i + \frac{\partial \Pi_H^*}{\partial \omega_i}\delta\omega_i + \frac{\partial \Pi_H^*}{\partial \varphi}\delta\varphi + \frac{\partial \Pi_H^*}{\partial s_i}\delta s_i = 0 \tag{39}$$

where

$$\Pi_H^* = \Pi_H^*(e(u), k(\omega), u, \omega, E(\varphi), s) = \Pi_H + \int_V s_k\big(\varepsilon_{ijk} u_{j,i} - 2\omega_k\big)\, dV \tag{40}$$

In Darrall et al. (2014), it is shown by deriving the corresponding Euler-Lagrange equations that the solutions to the variational problem of (39) satisfy linear and angular momentum balances, rotation-displacement compatibility, and force and moment traction boundary conditions. Following the same derivations as in Darrall et al. (2014), it is a simple task to show that evaluating the third term of (39) will also produce Euler-Lagrange equations corresponding to Gauss' law in differential form, (19), and the natural boundary conditions corresponding to (21).

Before developing the corresponding finite element formulation in the next section, we should emphasize the differences first developed in Hadjesfandiari (2014) between the present size-dependent piezoelectric theory and the prevailing flexoelectric version. In particular, the present

theory is consistent with Maxwell's equations of electromagnetism and the self-consistent theory of couple stresses, while the latter satisfies neither of these essential conditions. Furthermore, the present theory predicts that only two additional parameters, l and $\breve{f}$, appear for isotropic or centrosymmetric cubic materials, rather than three as required for the predominant flexoelectric theory. In this regard, we point to the difficulties expressed by Zubko et al. (2007) in estimating these three material parameters for cubic $SrTiO_3$ single crystals. Several statements in Zubko et al., (2007) suggest that perhaps the three flexoelectric material parameters are not independent. Two recent reviews on flexoelectricity express further concerns relating to the prevailing theory (Zubko et al., 2013; Yudin and Tagantsev, 2013). Thus, further physical and computational experiments are needed to clarify the underlying theory. The finite element formulation to be developed in the following section can be quite useful for those investigations.

3. Couple-stress piezoelectric finite element formulation

As with most continuum theories, the analytical solutions that are available are limited to very simple geometry and boundary conditions. Clearly numerical formulations must be developed in order to analyze real world problems that arise in the design process of modern technologies looking to take advantage of size-dependent piezoelectric effects. In this section a finite element formulation is developed for linear, centrosymmetric cubic and isotropic, piezoelectric solids based on the size-dependent theory of Hadjesfandiari (2013, 2014).

Voigt notation is used in this section for the purpose of simplifying calculations and programming. This means that the strain, $\boldsymbol{e}$, is represented by a vector rather than a second order tensor, and the constitutive tensor, $\boldsymbol{c}$, is expressed as a two-dimensional matrix rather than a fourth order tensor. For the two-dimensional, plane-strain, linear problems that we will explore here, we then have the following representations:

$$\boldsymbol{e} = \begin{bmatrix} e_{xx} \\ e_{yy} \\ \gamma_{xy} \end{bmatrix} = \begin{bmatrix} \dfrac{\partial u_x}{\partial x} \\ \dfrac{\partial u_y}{\partial y} \\ \dfrac{\partial u_x}{\partial y} + \dfrac{\partial u_y}{\partial x} \end{bmatrix} \tag{41}$$

$$\boldsymbol{c} = \begin{bmatrix} c_{11} & c_{12} & 0 \\ c_{12} & c_{11} & 0 \\ 0 & 0 & c_{44} \end{bmatrix} \tag{42a}$$

which specializes as follows for the isotropic case

$$\boldsymbol{c} = \frac{E(1-\nu)}{(1+\nu)(1-2\nu)}\begin{bmatrix} 1 & \frac{\nu}{1-\nu} & 0 \\ \frac{\nu}{1-\nu} & 1 & 0 \\ 0 & 0 & \frac{1-2\nu}{2(1-\nu)} \end{bmatrix} \tag{42b}$$

Here u_x is the component of displacement in the x-direction and u_y is the component of the displacement in the y-direction. Additionally, E is the Young's modulus, and ν is the Poisson's ratio. For plane-stress problems, only the matrix $\boldsymbol{c}$ will need to change (Bathe, 1996).

For planar problems, the engineering mean curvature vector can be written in terms of the one out of plane component of rotation, ω, explicitly as

$$\boldsymbol{k} = \begin{bmatrix} k_x \\ k_y \end{bmatrix} = \begin{bmatrix} -\frac{\partial \omega}{\partial y} \\ \frac{\partial \omega}{\partial x} \end{bmatrix} \tag{43}$$

The couple-stress constitutive matrix for linear centrosymmetric cubic and isotropic materials is

$$\boldsymbol{b} = 4\eta \begin{bmatrix} 1 & 0 \\ 0 & 1 \end{bmatrix} \tag{44}$$

while the corresponding piezoelectric-curvature coupling tensor, $\boldsymbol{\gamma}$, becomes

$$\boldsymbol{\gamma} = 2\,\check{f} \begin{bmatrix} 1 & 0 \\ 0 & 1 \end{bmatrix} \tag{45}$$

From (16), we can express the electric field in terms of the electric potential as

$$\boldsymbol{E} = \begin{bmatrix} E_x \\ E_y \end{bmatrix} = \begin{bmatrix} -\frac{\partial \varphi}{\partial x} \\ -\frac{\partial \varphi}{\partial y} \end{bmatrix} \tag{46}$$

We now consider the variational principle posed in the previous section. In vector notation, we have

$$\delta \Pi_H^* = 0 = \frac{\partial \Pi_H^*}{\partial \boldsymbol{u}} \delta \boldsymbol{u} + \frac{\partial \Pi_H^*}{\partial \boldsymbol{\omega}} \delta \boldsymbol{\omega} + \frac{\partial \Pi_H^*}{\partial \varphi} \delta \varphi + \frac{\partial \Pi_H^*}{\partial \boldsymbol{s}} \delta \boldsymbol{s} \tag{47}$$

where

$$\begin{aligned} \Pi_H^* = \frac{1}{2}\int_V \boldsymbol{e}^T \boldsymbol{c}\boldsymbol{e}\, dV + \frac{1}{2}\int_V \boldsymbol{k}^T \boldsymbol{b}\boldsymbol{k}\, dV + \int_V (curl\, \boldsymbol{u} - 2\boldsymbol{\omega})^T\, \boldsymbol{s}\, dV - \frac{1}{2}\int_V \boldsymbol{E}^T \boldsymbol{\varepsilon}\boldsymbol{E}\, dV - \int_V \boldsymbol{E}^T \boldsymbol{\gamma}\boldsymbol{k}\, dV \\ - \int_V \boldsymbol{u}^T \overline{\boldsymbol{F}}\, dV + \int_V \varphi \bar{\rho}_E\, dV - \int_{S_t} \boldsymbol{u}^T \bar{\boldsymbol{t}}\, dS - \int_{S_m} \boldsymbol{\omega}^T \bar{\boldsymbol{m}}\, dS - \int_{S_d} \varphi \bar{d}\, dS \end{aligned} \tag{48}$$

Next, we consider discretizing the domain into finite elements. Figure 1 shows the 8-node isoparametric quadrilateral master element used in the present formulation. This element has natural coordinates represented by r and s, with values for each element ranging from -1 to +1 in either direction. In the global coordinate system, here represented in two dimensions by normal Cartesian coordinates x and y, our element can take on any arbitrary shape, limited only by the need to maintain a well-defined Jacobian (Bathe, 1996; Zienkiewicz and Taylor, 2000).

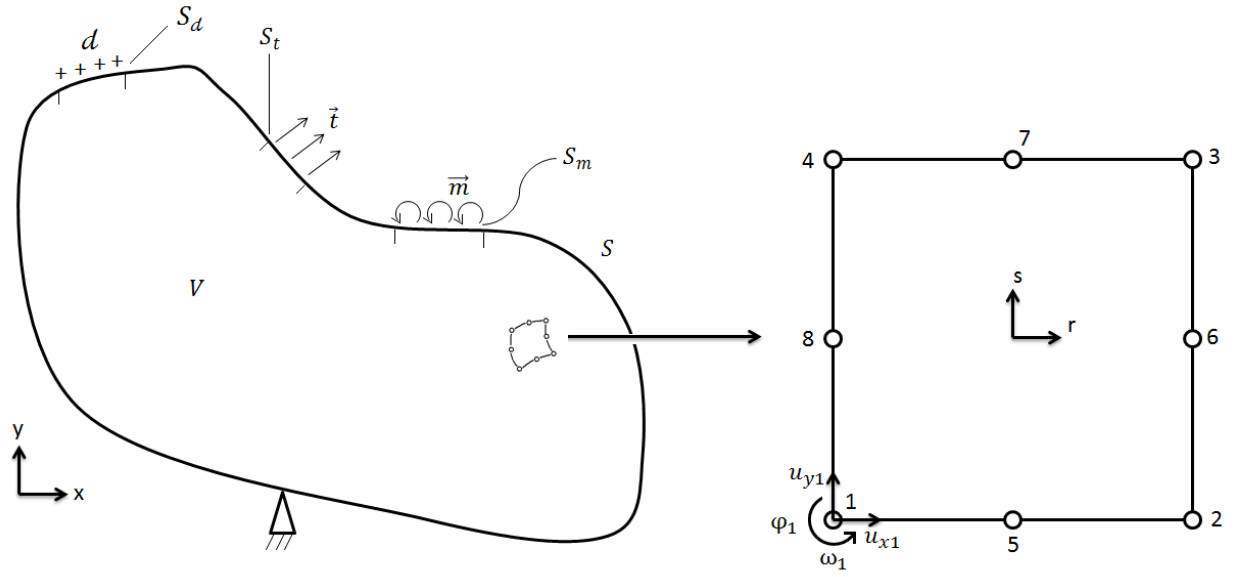

Fig. 1. General planar body and sample 8-node master element

Standard serendipity quadratic shape functions $\boldsymbol{N}$ (Zienkiewicz and Taylor, 2000; Bathe, 1996) are used in this formulation, where

$$\boldsymbol{N}^T = \begin{bmatrix} \frac{1}{4}(1-r)(1-s) - \frac{1}{4}(1-s^2)(1-r) - \frac{1}{4}(1-r^2)(1-s) \\ \frac{1}{4}(1+r)(1-s) - \frac{1}{4}(1-r^2)(1-s) - \frac{1}{4}(1-s^2)(1+r) \\ \frac{1}{4}(1+r)(1+s) - \frac{1}{4}(1-r^2)(1+s) - \frac{1}{4}(1-s^2)(1+r) \\ \frac{1}{4}(1-r)(1+s) - \frac{1}{4}(1-r^2)(1+s) - \frac{1}{4}(1-s^2)(1-r) \\ \frac{1}{2}(1-s)(1-r^2) \\ \frac{1}{2}(1+r)(1-s^2) \\ \frac{1}{2}(1+s)(1-r^2) \\ \frac{1}{2}(1-r)(1-s^2) \end{bmatrix} \tag{49}$$

These same shape functions, $\boldsymbol{N}$, are used to interpolate both the geometric coordinates of the element as well as the displacement, rotation, and electric potential within an element. This means that we can represent the geometry of an arbitrary shaped element in terms of the element natural coordinates r and s via the following relations

$$x \cong \boldsymbol{N}\hat{\boldsymbol{x}} \tag{50a}$$

$$y \cong \boldsymbol{N}\hat{\boldsymbol{y}} \tag{50b}$$

where $\hat{\boldsymbol{x}}$ and $\hat{\boldsymbol{y}}$ are the global coordinate values of nodes 1 through 8 for any particular element. In general the hat notation is used to represent vectors containing quantities at nodes 1 through 8. Then, for our discretized approximation for displacement, rotation, and electric potential within an element, we have

$$u_x \cong \boldsymbol{N}\hat{\boldsymbol{u}}_{\boldsymbol{x}} \tag{51a}$$

$$u_y \cong \boldsymbol{N}\hat{\boldsymbol{u}}_{\boldsymbol{y}} \tag{51b}$$

$$\omega \cong \boldsymbol{N}\hat{\boldsymbol{\omega}} \tag{52}$$

$$\varphi \cong \boldsymbol{N}\hat{\boldsymbol{\varphi}} \tag{53}$$

For the displacements, rotations, and electric potential on the boundaries S_t, S_m, and S_d we will need to use surface interpolation functions, such that

$$u_{xS_t} \cong \boldsymbol{N}_S\hat{\boldsymbol{u}}_{\boldsymbol{x}} \tag{54}$$

$$u_{yS_t} \cong \boldsymbol{N}_S\hat{\boldsymbol{u}}_{\boldsymbol{y}} \tag{55}$$

$$\omega_{S_m} \cong \boldsymbol{N}_{\boldsymbol{S}}\hat{\boldsymbol{\omega}} \tag{56}$$

$$\varphi_{S_d} \cong \boldsymbol{N}_{\boldsymbol{S}}\hat{\boldsymbol{\varphi}} \tag{57}$$

For a 2-d body these surface shape functions can be expressed in terms of one natural coordinate, r, as follows

$$\boldsymbol{N}_{\boldsymbol{S}}^T = \begin{bmatrix} \frac{1}{2}(1-r) - \frac{1}{2}(1-r^2) \\ \frac{1}{2}(1+r) - \frac{1}{2}(1-r^2) \\ 1-r^2 \end{bmatrix} \tag{58}$$

The strains, curvatures, and electric field in (48) can now be replaced with approximate discrete representations in terms of displacements, rotations, and electric potential, respectively. To do this we must introduce new matrices, the strain-displacement matrix, $\boldsymbol{B}_{\boldsymbol{e}}$, such that

$$\boldsymbol{e} \cong \boldsymbol{B}_{\boldsymbol{e}}\hat{\boldsymbol{u}} \tag{59}$$

where $\hat{\boldsymbol{u}}$ is a concatenated vector with 16 values that contains both the horizontal and vertical components of displacements in the following form

$$\hat{\boldsymbol{u}}^T = [\hat{\boldsymbol{u}}_{\boldsymbol{x}}, \hat{\boldsymbol{u}}_{\boldsymbol{y}}] = [\ \hat{u}_{x1} \quad \hat{u}_{y1} \quad \ldots \quad \hat{u}_{x8} \quad \hat{u}_{y8}\ ] \tag{60}$$

Also we have the curvature-rotation matrix, $\boldsymbol{B}_{\boldsymbol{k}}$, such that

$$\boldsymbol{k} \cong \boldsymbol{B}_{\boldsymbol{k}}\hat{\boldsymbol{\omega}} \tag{61}$$

and the curl-displacement matrix, $\boldsymbol{B}_{\boldsymbol{curl}}$, such that

$$\nabla \times \boldsymbol{u} \cong \boldsymbol{B}_{\boldsymbol{curl}}\hat{\boldsymbol{u}} \tag{62}$$

and finally the electric field-potential matrix, $\boldsymbol{B}_{\boldsymbol{E}}$, such that

$$\boldsymbol{E} \cong \boldsymbol{B}_{\boldsymbol{E}}\hat{\boldsymbol{\varphi}} \tag{63}$$

For the planar problems in this paper we can write out these $\boldsymbol{B}$ matrices explicitly as follows:

$$\boldsymbol{B_e} = \begin{bmatrix} \frac{\partial N_1}{\partial x} & 0 & & \frac{\partial N_8}{\partial x} & 0 \\ 0 & \frac{\partial N_1}{\partial y} & \dots & 0 & \frac{\partial N_8}{\partial y} \\ \frac{\partial N_1}{\partial y} & \frac{\partial N_1}{\partial x} & & \frac{\partial N_8}{\partial y} & \frac{\partial N_8}{\partial x} \end{bmatrix} \tag{64}$$

$$\boldsymbol{B_k} = \begin{bmatrix} -\frac{\partial N_1}{\partial y} & \dots & -\frac{\partial N_8}{\partial y} \\ \frac{\partial N_1}{\partial x} & & \frac{\partial N_8}{\partial x} \end{bmatrix} \tag{65}$$

$$\boldsymbol{B_{curl}} = \begin{bmatrix} -\frac{\partial N_1}{\partial y} & \frac{\partial N_1}{\partial x} & \dots & -\frac{\partial N_8}{\partial y} & \frac{\partial N_8}{\partial x} \end{bmatrix} \tag{66}$$

$$\boldsymbol{B_E} = \begin{bmatrix} -\frac{\partial N_1}{\partial x} & -\frac{\partial N_2}{\partial x} & \dots & -\frac{\partial N_7}{\partial x} & -\frac{\partial N_8}{\partial x} \\ -\frac{\partial N_1}{\partial y} & -\frac{\partial N_2}{\partial y} & & -\frac{\partial N_7}{\partial y} & -\frac{\partial N_8}{\partial y} \end{bmatrix} \tag{67}$$

Here $\boldsymbol{B_e}$ will be a matrix of size $[3 \times 16]$, $\boldsymbol{B_k}$ will be a matrix of size $[2 \times 8]$, $\boldsymbol{B_{curl}}$ will be a matrix of size $[1 \times 16]$, and $\boldsymbol{B_E}$ will be a matrix of size $[2 \times 8]$. For all cases, the $\boldsymbol{B}$ matrices above are functions of the first derivatives of the shape functions with respect to global Cartesian coordinates, x and y.

Finally, we must also consider the discrete approximation of the skew-symmetric stress pseudo vector. For 2-d problems this vector actually simplifies to one component in the out of plane direction. Further simplifying matters, we need only C^{-1} continuity in this formulation and therefore consider $\boldsymbol{s}$ to be constant throughout each element.

Now, upon substitution of the discrete representations of our variables into (48), and then taking the first variation with respect to the discrete variables, we are left with the following for each element

$$\begin{aligned} \delta\Pi_H^* = 0 = (\delta\hat{\boldsymbol{u}})^T & \left[\int_V (\boldsymbol{B}^T\boldsymbol{c}\boldsymbol{B})\,\hat{\boldsymbol{u}}\,J_d dV + \int_V \boldsymbol{B_{curl}}^T\,\boldsymbol{s}\,J_d\,dV - \int_V \boldsymbol{N}^T\bar{\boldsymbol{F}}\,J_d dV - \int_{S_t} \boldsymbol{N}_S^T\bar{\boldsymbol{t}}\,J_{dS}\,dS\right] \\ & + (\delta\hat{\boldsymbol{\omega}})^T\left[\int_V (\boldsymbol{B_k}^T\boldsymbol{b}\boldsymbol{B_k})\,\hat{\boldsymbol{\omega}}\,J_d dV - \int_V (\boldsymbol{B_k}^T\boldsymbol{\gamma}\boldsymbol{B_E})\,\hat{\boldsymbol{\varphi}}\,J_d dV\right. \\ & \left. + \int_V -2\boldsymbol{N}^T\boldsymbol{s}\,J_d dV - \int_{S_m} \boldsymbol{N}_S^T\,\bar{\boldsymbol{m}}\,J_{dS}\,dS\right] + (\delta\boldsymbol{s})\left[\int_V (\boldsymbol{B_{curl}}\hat{\boldsymbol{u}} - 2\boldsymbol{N}\hat{\boldsymbol{\omega}})\,J_d dV\right] \\ & + (\delta\hat{\boldsymbol{\varphi}})^T\left[-\int_V (\boldsymbol{B_E}^T\boldsymbol{\varepsilon}\boldsymbol{B_E})\,\hat{\boldsymbol{\varphi}}\,J_d dV - \int_V (\boldsymbol{B_E}^T\boldsymbol{\gamma}\boldsymbol{B_k})\,\hat{\boldsymbol{\omega}}\,J_d dV + \int_V \boldsymbol{N}^T\bar{\rho}_E\,dV - \int_{S_\sigma} \boldsymbol{N}_S^T\,\bar{d}\,dS\right] \end{aligned} \tag{68}$$

where J_d and J_{dS} represent the determinants of the Jacobian of the volume and the surface of an element, respectively. For the integration over the 8-noded isoparametric size-dependent

piezoelectric elements presented here, standard 3×3 point Gauss quadrature is used (Bathe, 1996; Zienkiewicz and Taylor, 2000).

Due to the fact that the variational factors, $\delta\hat{\boldsymbol{u}}$, $\delta\hat{\boldsymbol{\omega}}$, $\delta\hat{\boldsymbol{\varphi}}$, and $\delta\boldsymbol{s}$ have arbitrary value, the four terms in square brackets above all must be identically zero for this equation to be valid. This provides us with four coupled sets of linear algebraic equations for each element. These are our final finite element equations for a single element in matrix form.

We now have a set of linear algebraic equations for each element. Here we choose to organize these element equations into the form shown in Fig. 2.

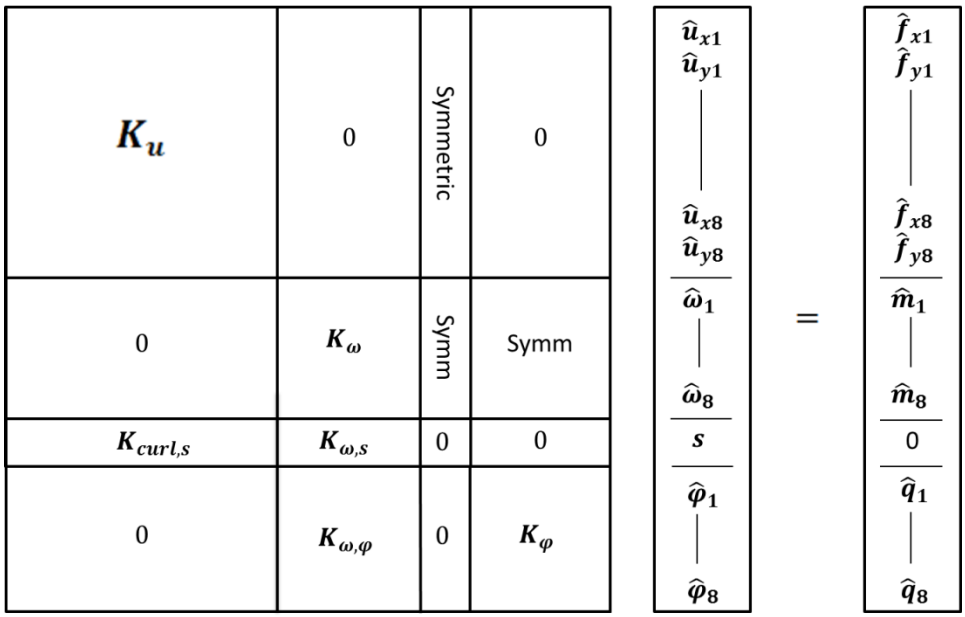

Fig. 2. Structure of resulting element equations before assembly

Corresponding to (68), the stiffness terms on the left hand side are calculated explicitly as follows:

$$\boldsymbol{K_u} = \int_V (\boldsymbol{B}^T \boldsymbol{C} \boldsymbol{B})\, J_d dV \tag{69a}$$

$$\boldsymbol{K_\omega} = \int_V (\boldsymbol{B_k^T} \boldsymbol{b} \boldsymbol{B_k})\, J_d dV \tag{69b}$$

$$\boldsymbol{K_{curl,s}} = \int_V (\boldsymbol{B_{curl}})\, J_d dV \tag{69c}$$

$$\boldsymbol{K_{\omega,s}} = -\int_V (2\boldsymbol{N})\, J_d dV \tag{69d}$$

$$\boldsymbol{K_{\omega,\varphi}} = -\int_V (\boldsymbol{B_E^T} \boldsymbol{\gamma} \boldsymbol{B_k})\, J_d dV \tag{69e}$$

$$\boldsymbol{K_\varphi} = -\int_V (\boldsymbol{B_E^T} \boldsymbol{\varepsilon} \boldsymbol{B_E})\, J_d dV \tag{69f}$$

Meanwhile, for the right hand side, we have

$$\hat{\boldsymbol{f}}_{\boldsymbol{x}} = \int_V \boldsymbol{N}^T \bar{F}_x \, J_d dV + \int_{S_t} \boldsymbol{N}_S^T \, \bar{t}_x \, J_{dS} \, dS \tag{70a}$$

$$\hat{\boldsymbol{f}}_{\boldsymbol{y}} = \int_V \boldsymbol{N}^T \bar{F}_y \, J_d dV + \int_{S_t} \boldsymbol{N}_S^T \, \bar{t}_y \, J_{dS} \, dS \tag{70b}$$

$$\hat{\boldsymbol{m}} = \int_{S_m} \boldsymbol{N}_S^T \, \bar{m} \, J_{dS} \, dS \tag{70c}$$

$$\hat{\boldsymbol{q}} = -\int_V \boldsymbol{N}^T \bar{\rho}_E \, J_d dV + \int_{S_d} \boldsymbol{N}_S^T \, \bar{d} \, J_{dS} dS \tag{70d}$$

where the subscripts x and y above indicate the components of force in that respective direction. All terms that appear in the right hand side are of course known quantities, as indicated by the overbars in (70a-d).

After evaluating the stiffness matrix and forcing vector on the element level, we then follow standard finite element procedures (Bathe, 1996; Zienkiewicz and Taylor, 2000) to assemble and solve the global set of linear algebraic equations

$$\boldsymbol{K}\boldsymbol{u} = \boldsymbol{f} \tag{71}$$

where now $\boldsymbol{u}$ includes all nodal values for displacement, rotation, and electric potential, along with the element-based skew-symmetric stress.

Before considering the solution to several boundary value problems, two additional points should be made. The first relates to the introduction of the skew-symmetric stress Lagrange multipliers to enforce the displacement-rotation constraint. Notice that the corresponding diagonal block of the stiffness matrix displayed in Fig. 2 becomes zero and, as a consequence, the overall system matrix in (71) is indefinite. Consequently, sophisticated direct solvers appropriate for sparse, symmetric, indefinite matrices are needed to maintain accuracy of the solution. In the present work, the MATLAB (2014) implementation of the unsymmetric multifrontal sparse LU factorization package UMFPACK is used with a symmetric pivoting strategy (Davis and Duff, 1997; Davis, 2004).

The second point relates to Dirichlet boundary conditions that must be enforced on surfaces with fixed non-zero displacement, rotation, and/or electric potential. There are many ways to do this. One simple approach is to replace the corresponding right hand side component with the specified boundary value and then multiply both the corresponding diagonal and right hand side components by a sufficiently large penalty parameter. However, due to the sensitive nature of the indefinite system equations associated with the present formulation, we prefer to avoid penalty parameters. Instead, we modify the right hand side by subtracting the product of the columns corresponding to the specified nodal degrees of freedom and the enforced boundary value. Then, the corresponding rows and columns can be zeroed, while the diagonal value is set to unity and the corresponding right hand side entry is equated to the desired value of displacement, rotation, or electric potential.

4. Boundary value problems

4.1 Long isotropic cylinder with constant applied electric field on the surface

For this problem we consider a long, isotropic, circular cylinder with radius a. The surface of the cylinder is exposed to an applied constant electric field of magnitude E_0 directed in the positive x-direction. This serves as a direct Dirichlet boundary condition on the electric potential. Clearly from (16) the boundary condition for electric potential will be

$$\varphi = -E_0 a \cos\theta \tag{72}$$

on surface $r = a$.

The other boundary conditions for this problem are zero force- and moment-tractions on the surface, along with constrained displacement and rotation of the center point. The problem geometry may also be simplified by enforcing certain symmetry boundary conditions along the horizontal and vertical axes. Specifically, the boundary conditions for the vertical axis are zero electric potential, zero vertical displacement, zero horizontal force-traction, and zero moment-traction. The boundary conditions for the horizontal axis are zero normal electric displacement, zero vertical displacement, zero horizontal force-traction, and zero moment-traction. By enforcing these boundary conditions only the first quadrant of the cylinder geometry needs to be considered.

For material properties in dimensionless form we consider $E = 5/2$, $\nu = 1/4$, and $\varepsilon = 1$. The magnitude of the applied electric field is considered unity for all simulations here. An unstructured mesh with 126 elements is used.

The problem has an analytical solution derived in Hadjesfandiari (2013) that will be used to validate the numerical solutions here. Displacement results are presented in Table 1, where U_0 is the horizontal displacement at the point on the surface at $\theta = 0$, and U_{90} is the horizontal displacement at the point on the surface at $\theta = \pi/2$. From Table 1, we see that the numerical solutions are in excellent agreement with the analytical solution.

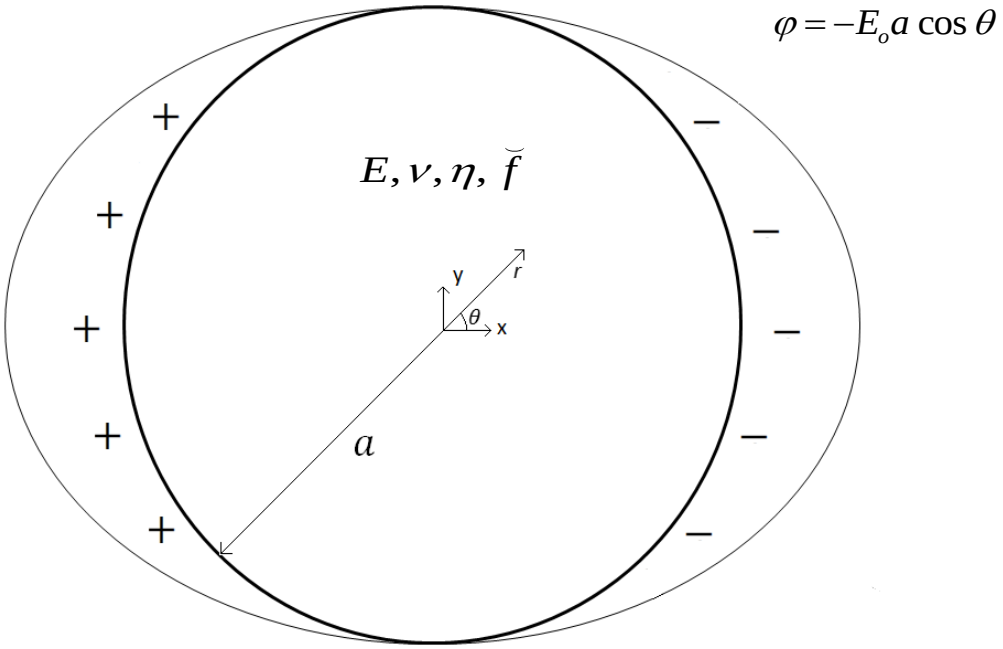

Fig. 3. Long cylinder with constrained potential on surface

Table 1. Results for long cylinder with constant applied electric field on surface

$\breve{f}$	η	Analytical (Hadjesfandiari, 2013)		FE (126 elements)		Relative Error: $\frac{U_{FE} - U_{analytic}}{U_{analytic}}$	
		U_{90}	U_0	U_{90}	U_0	U_{90}	U_0
0	0.1	0	0	0	0	0	0
0.01	0.1	0.0156683	0.0016525	0.0156677	0.0016488	-3.63E-05	-2.21E-03
0.1	0.1	0.1566826	0.0165248	0.1566769	0.0164883	-3.63E-05	-2.21E-03
1	0.1	1.5668259	0.1652484	1.5667691	0.1648831	-3.63E-05	-2.21E-03
0.1	0.01	0.2647973	0.0099273	0.2642131	0.0096449	-2.21E-03	-2.84E-02
0.1	1	0.0311736	0.0042998	0.0311788	0.0042982	1.68E-04	-3.74E-04

4.2 Long isotropic cantilever in constant vertical electric field (normalized parameters)

Here we consider a long, isotropic cantilever with a constant electric potential applied to the top and bottom surfaces. The upper surface can be considered grounded with $\varphi = 0$ and the bottom surface is held at a value of $\varphi = h$. Note that again we are considering all quantities to be dimensionless here. These conditions on the potential will produce a unit uniform constant electric field in the positive y- direction, which in turn induces curvature in the beam. This problem is useful for exploring both the direct connection between electric field and curvature present in consistent couple stress piezoelectricity, and the size-dependency of the electromechanical phenomena. This problem also has significance to the development of small

scale sensors and actuators. From the above problem definition, the vertical electric field can be calculated by

$$E_y \cong \frac{\varphi_{bottom}-\varphi_{top}}{h} = \frac{\Delta\varphi}{h} = 1 \tag{73}$$

The material parameters in non-dimensional form for this beam are as follows: $E = 2$, $l = 1$, $\breve{f} = 1$, $\varepsilon = 1$ and $\nu = 0$. Aside from the electric potential boundary condition specified on the top and bottom surface, the following boundary conditions are enforced; there is no applied force- or moment-tractions, the left and right hand sides are considered to be electrically insulated such that $d = 0$, and finally the vertical displacements, horizontal displacements, and the rotations on the surface with $x = 0$ are constrained to be zero.

The mesh used here consists of rectangular elements arranged such that there are $20N$ elements lengthwise and $2N$ elements transversely. The finest mesh had $N = 8$ and therefore consisted of 2,560 elements. Figure 5 shows excellent convergence of the vertical end displacement, U_y, with uniform mesh refinement for the case with $h/l = 1$. For the numerical experiments with results presented in Figs. 6 and 7, the characteristic geometry, h, was varied in order to show the size-dependency of the theory.

For a long slender beam, such as the one examined here, we expect the assumptions of an Euler-Bernoulli beam model to hold true. Recently, an Euler-Bernoulli beam model based on the consistent size-dependent piezoelectric theory presented in Hadjesfandiari (2013) was derived in Li et al. (2014). From this paper the vertical displacements of the beam should be:

$$u_y(x) \approx \frac{b\breve{f}\Delta\varphi}{\frac{EI}{2} + 2Gl^2A}x^2 \tag{74}$$

where b is the beam depth, I is the area moment of inertia, and A is the cross sectional area. This solution corresponds to constant curvature in the y-direction. The induced curvature however is clearly size-dependent. For small scales ($h/l < 1$) we expect the term involving the couple-stress parameter to limit the induced curvature such that:

$$k_y \approx \frac{b\breve{f}\Delta\varphi}{2Gl^2A} = \frac{\breve{f}E_y}{2Gl^2} \tag{75}$$

For larger scales ($h/l \gg 1$), we expect the classical bending stiffness term to limit the induced curvature such that:

$$k_y \approx \frac{b\breve{f}\Delta\varphi}{EI/2} = \frac{24\breve{f}E_y}{Eh^2} \tag{76}$$

The results using the FE formulation developed here show that indeed the solution to this problem is a field with constant k_y, with the exception of minor edge effects at the right boundary. The solutions are in excellent agreement with equations (74) through (76). From Fig. 6, we see that for very small characteristic geometry $(h/l < 1)$ we have for the induced curvature, $k_y = \check{f}\, E_y/2Gl^2$. For increasing characteristic geometry starting from $h/l \approx 10$, we note that k_y decreases proportional to $1/h^2$, as expected from (76). This size-dependent behavior leads to some maximum end displacement that is possible for this size-dependent piezoelectric problem. This is very interesting because it means that even for very large geometries we will still have some displacement that is not dependent on the cantilever geometry. In other words even for large scales the size-dependent piezoelectric effect is non-zero. However, as one can see from Fig. 7, the ratio of the vertical end displacement at point A to the cantilever geometry, U_y/L, is decreasing proportional to $1/h$. Then, for larger length scales, we can conclude that the deformation due to the size-dependent piezoelectric effect, although equal to some nonzero value, will become negligible and perhaps even impossible to detect. Also from Fig. 7, we see that the size-dependent piezoelectric effects relative to size of the cantilever are greatest for $h/l \approx 5$. We should note that generally results will deviate from (74) for real materials due to non-zero Poisson's ratio. The formulation developed here is capable of accurately modeling this effect too.

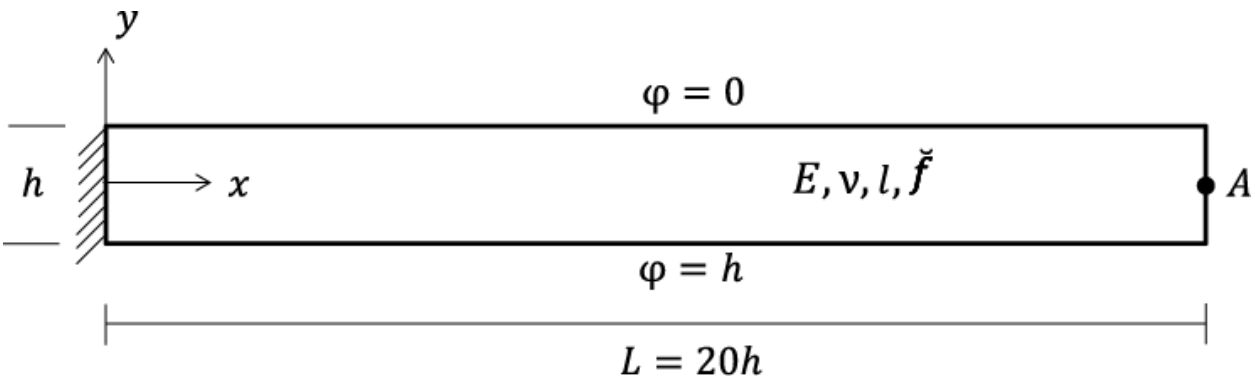

Fig. 4. Schematic of size-dependent piezoelectric cantilever

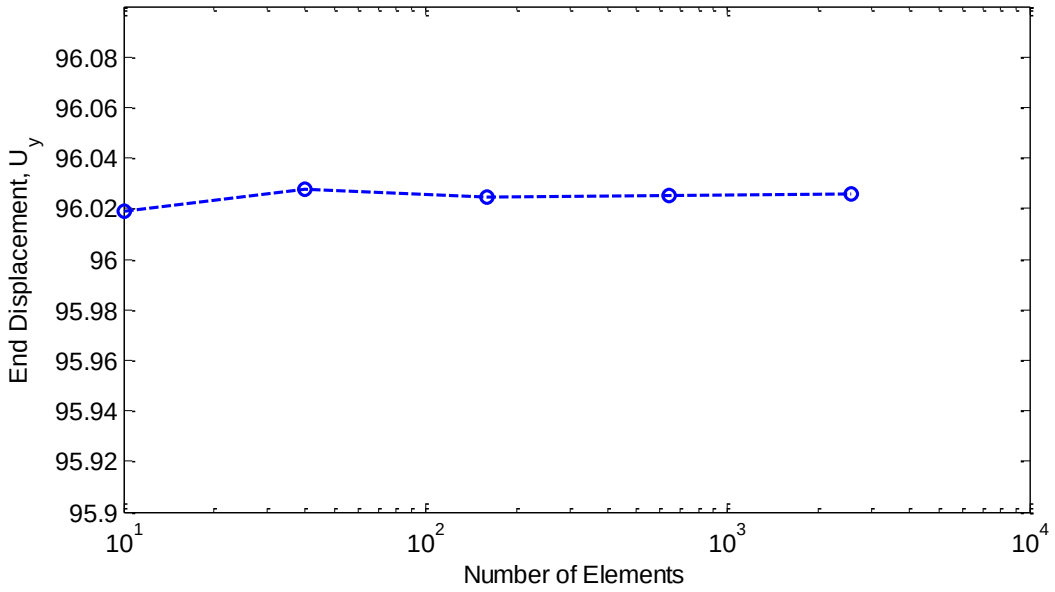

Fig. 5. Convergence of end displacement with mesh refinement

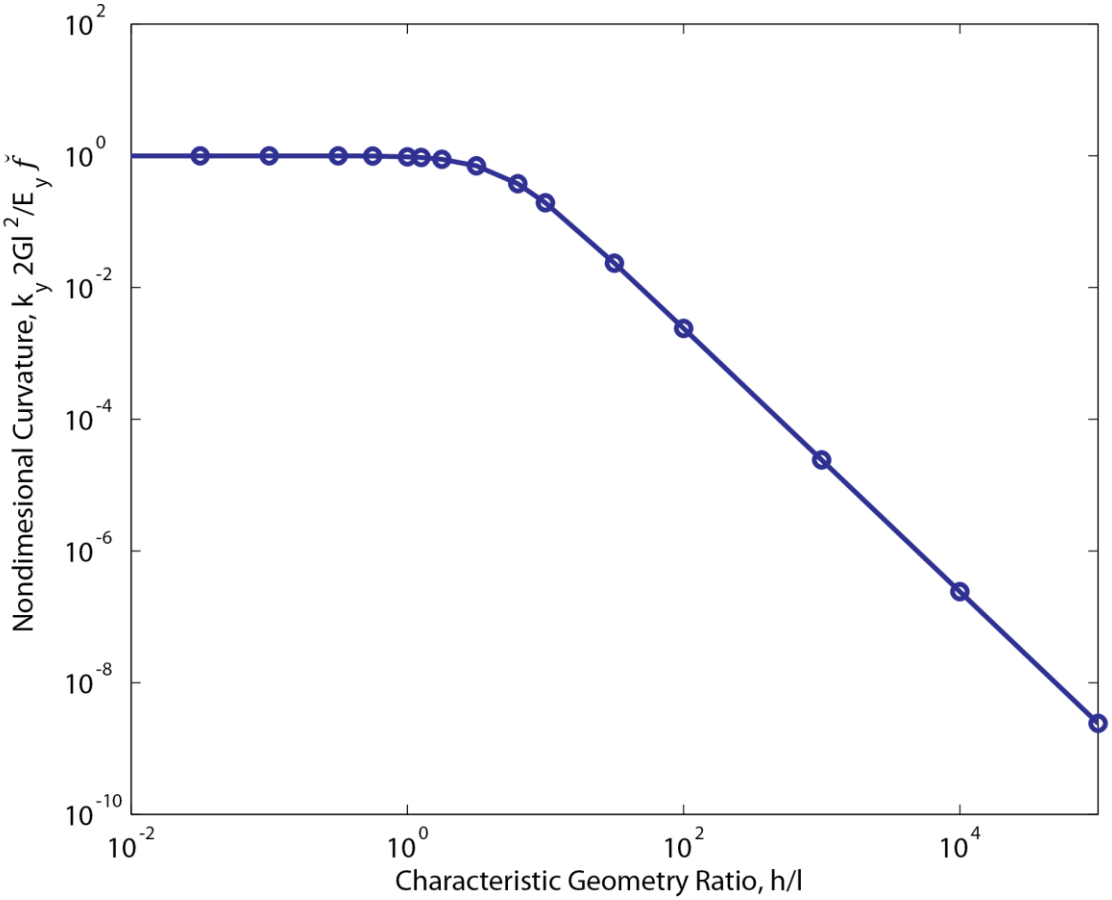

Fig. 6. Nondimensionalized curvature with scaling of cantilever geometry

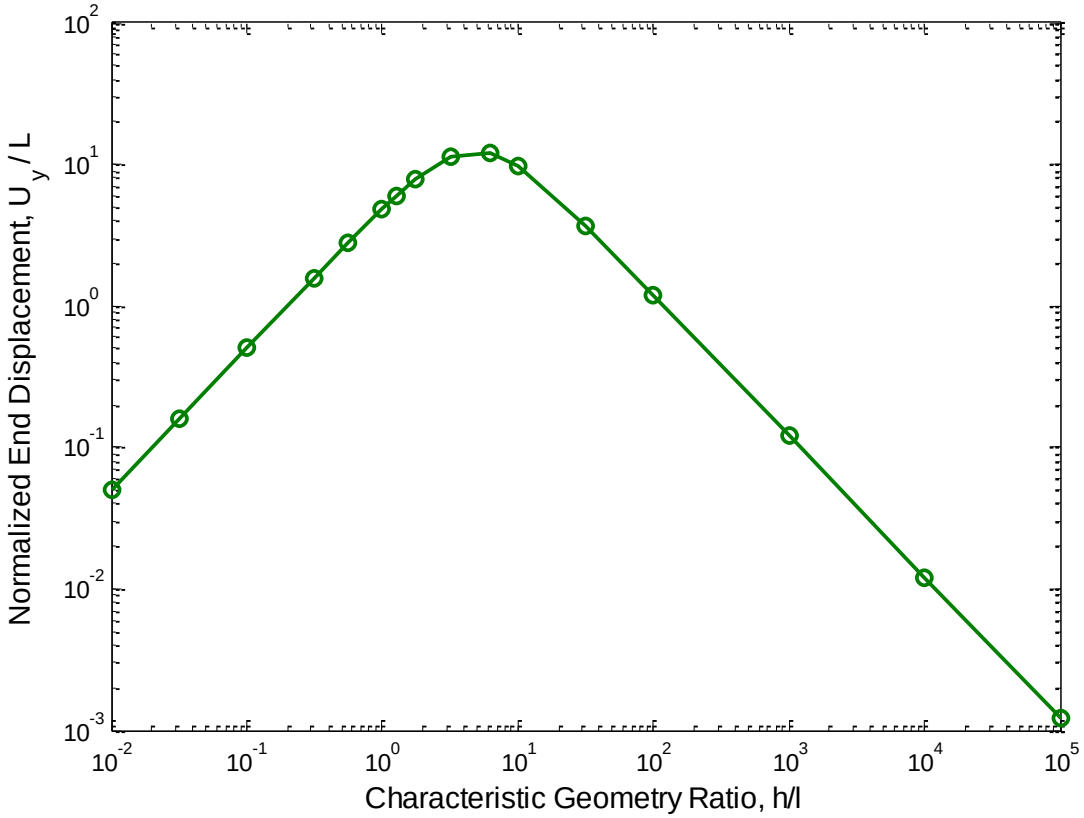

Fig. 7. Ratio of end displacement to length with scaling of cantilever geometry

Finally, we should note that Figs. 6 and 7 include results for $h/l < 1$. With limited experimental data available at this time to estimate the couple-stress parameter size-dependent l, it is not certain that continuum mechanics theories are applicable for length scales in that range. In any case, we believe that it is appropriate to explore the interesting phenomena that size-dependent piezoelectric theory predicts on these minute length scales.

4.3 Long cantilever in constant vertical electric field (Barium Titanate ceramic)

In this section, we analyze a cantilever with the same geometry and boundary conditions as described in the previous section. However, now we consider the material to be Barium Titanate ceramic ($BaTiO_3$) at room temperature, which in single crystal form has cubic centrosymmetric structure. The same mesh from the previous section was used. The beam has characteristic dimension of $h = 1\mu m$ and correspondingly, $L = 20\ \mu m$. The piezoelectric-curvature parameter was approximated based on experiments by Ma and Cross (2006). The other material properties used here were tabulated in Jaffe et al. (1971) and originally measured by Bechmann (1956). As noted above, in single crystal form, this material is centrosymmetric cubic. Based on the

measured elastic properties, however, it is clear that the material is not far from being isotropic. As such, for $BaTiO_3$ ceramic, we approximate isotropic elastic coefficients by making the assumption that $G = c_{44}$, $\nu = 0.325$ and then use Hooke's law for isotropic material to calculate an effective Young's modulus. All material properties used here are tabulated in Table 2.

The cantilever was subject to a uniform vertical electric field of $E_y = 1\, V/\mu m$. The vertical end displacement, U_y, was plotted against h/l in Figure 8. Clearly for $BaTiO_3$ the size-dependent piezoelectric effect is not negligible, as an electric field of $1V/\mu m$ causes a vertical end displacement of $U_y \approx 0.4\ \mu m$ (for $h/l > 10$).

Table 2: Approximate $BaTiO_3$ material properties used in simulation

Piezoelectric-curvature parameter, $\check{f}\ (\mu C/\mu m)$	$\sim 10 \times 10^{-6}$
Young's Modulus, $E\ (N/\mu m^2)$	113.7×10^{-3}
Shear Modulus, $G\ (N/\mu m^2)$	42.9×10^{-3}
Permittivity, $\varepsilon\ (\mu C^2/N\mu m^2)$	1.239×10^{-8}

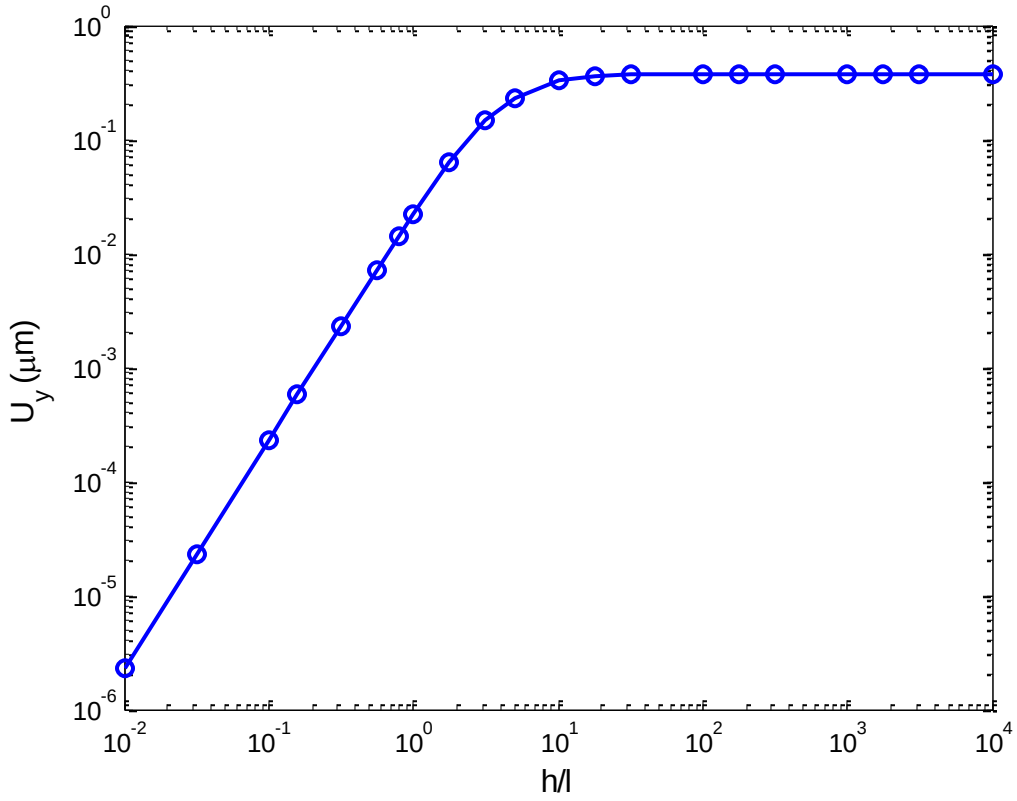

Fig. 8: Vertical end displacement with varying values of l

4.4 Long isotropic cantilever plate with transverse end-loading

This final problem analyzes the induced electric field in an isotropic cantilever subject to end loading under plane-strain conditions. The loading considered here is a transverse shear traction loading with a parabolic distribution. Figure 9 shows a schematic of the problem. The plate has thickness $2a$, where $a = 0.5$ here, and length $L = 20$. For all simulations, we consider the following dimensionless material properties; Young's modulus, $E = 5/2$, Poisson ratio, $\nu = 1/4$, and electric permittivity, $\varepsilon = 1$.

For boundary conditions we consider zero displacement on the left surface as well as zero electric potential at the origin. All surfaces are considered to be electrically insulated, such that $d = 0$, and also free of moment-tractions. The top and bottom surfaces are tractionless. Finally, the right surface of the plate has an applied shear traction with a parabolic profile, such that $t_y = t_0(1 - y^2/a^2)$.

Figure 10 shows a fill plot of the induced scalar electric potential field. The corresponding field is symmetric and has a maximum value on the top surface near the fixed surface at $x = 0$ and a minimum value on the bottom surface at that same end. Clearly a quantity of interest is the difference between the maximum and minimum value of electric potential. Figure 11 shows a convergence study of the maximum electric potential difference. A coarse mesh with ten rectangular elements was the original mesh. This coarse mesh was systematically refined by dividing each element into four equal sized rectangular elements. For the purpose of uniformity no localized mesh refinement was considered. Table 3 provides values of the maximum electric potential difference and the maximum end vertical displacement, U_y, for various values of the couple-stress and curvature-piezoelectric parameters for this example of the direct size-dependent piezoelectric effect in an isotropic material.

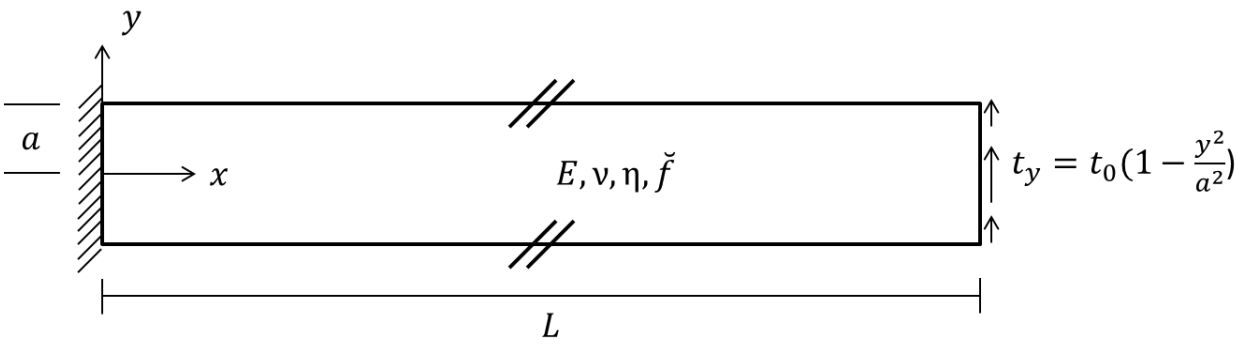

Fig. 9. Schematic of long cantilever plate

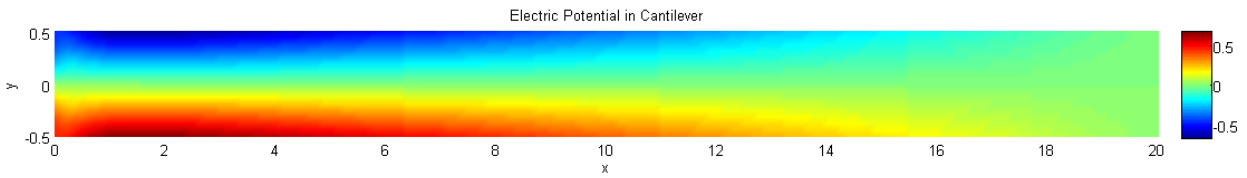

Fig. 10. Plot of electric potential field resulting from transverse loading ($\eta = 1,\ \check{f} = 1$)

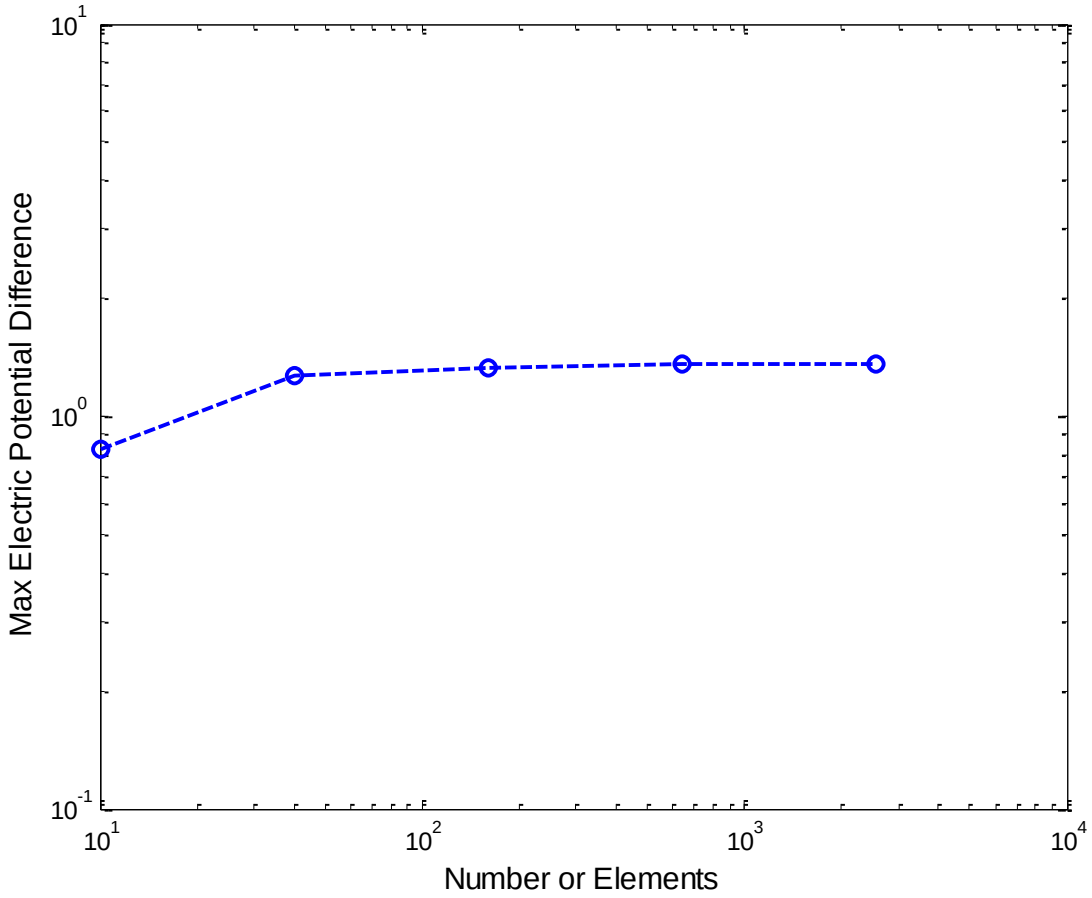

Fig. 11. Convergence of $(\varphi_{max} - \varphi_{min})$ with uniform mesh refinement ($\eta = 1,\ \check{f} = 1$)

Table 3. Results for long cantilever plate with transverse end loading, 2560 elements

$\check{f}$	η	$\varphi_{max} - \varphi_{min}$	$U_y \times 10^{-3}$
0.01	0.1	0.9395	7.2061
0.1	0.1	8.8229	6.8181
1	0.1	12.4577	1.6352
1	0.01	13.0643	2.0725
1	1	1.3632	1.6344

5. Conclusions

The size-dependent piezoelectricity developed in Hadjesfandiari (2013) provides a theory, which couples the electric field and mean curvatures in a manner that is consistent with Maxwell's equations of electromagnetism and skew-symmetric couple stress size-dependent mechanics. Based on this piezoelectric theory, and the mixed variational principle for size-dependent elasticity presented in Darrall et al. (2014), we have developed a mixed finite element formulation for planar couple stress piezoelectric problems in centrosymmetric cubic and isotropic media. This formulation uses Lagrange multipliers to explicitly enforce rotation-displacement compatibility, which reduces the variational problem from having a C^1 to a C^0 continuity requirement. The Lagrange multipliers conveniently are equal to the skew-symmetric portion of the force-stress tensor. However, the resulting system matrix becomes indefinite and care is needed to maintain accuracy in the solver.

The results from the cylinder problem illustrate the convergence characteristics of this formulation compared with an analytical solution for the converse size-dependent piezoelectric effect. Meanwhile, the problem of a cantilever in a uniform transverse electric field showed several interesting results of size-dependent piezoelectricity. For example, it was shown that indeed size-dependent piezoelectric effects are most significant for characteristic geometry on the order of the couple-stress length parameter, l. Also, it was found that at large scales, the size-dependent piezoelectric effects become negligible when compared to the characteristic geometric scale, but do not vanish completely. It was shown that the size-dependent piezoelectric effect is indeed significant for perovskite ceramics, such as Barium Titanate. The final problem illustrates the direct effect, in which an applied load induces an electric field.

Judging from the great impact that classical piezoelectricity has had on technology in the last fifty years, and the fact that new technology now is being developed on micro- and nano-length scales, it should be expected that modeling of piezoelectric phenomena at small scales will become increasingly important. Here we have restricted ourselves to consider only centrosymmetric cubic and isotropic materials, where although classical piezoelectric effects are not present, generally size-dependent piezoelectric effects can occur. Furthermore, while our present finite element formulation is for planar problems, the extensions to axisymmetric and general 3-d problems certainly are of interest. This is especially true in the latter case to enable the comparison with careful physical experiments on cubic single crystals to examine the theory. Thus, the current size-dependent piezoelectric finite element formulation and its extensions can be expected to provide an excellent tool for doing such analyses and potentially to influence future material, structure and device design over a broad range of applications.

References

Allik, H., Hughes, T.J.R., 1970. Finite element method for piezo-electric vibration. Int. J. Num. Meth. Engrg. 2, 151-157.

Baskaran, S., He, X.T., Chen, Q., Fu, J.Y., 2011. Experimental studies on the direct flexoelectric effect in α-phase polyvinylidene fluoride films. Appl. Phys. Lett. 98, 242901.

Bathe, K.J., 1996. Finite Element Procedures. Prentice Hall, Englewood Cliffs, N.J.

Bechmann, R., 1956. Elastic, piezoelectric, and dielectric constants of polarized barium titanate ceramics and some applicationso of the piezoelectric equations. J. Acoust. Soc. Am. 28, 347-50.

Benjeddou, A., 2000. Advances in piezoelectric finite element modeling of adaptive structural elements: a survey. Comput. Struct. 76, 347-363.

Buhlmann, S., Dwir, B., Baborowski, J., Muralt, P., 2002. Size effects in mesoscopic epitaxial ferroelectric structures: increase of piezoelectric response with decreasing feature-size. Appl. Phys. Lett. 80, 3195-3197.

Cady, W.G., 1964. Piezoelectricity: An Introduction to the Theory and Applications of Electro-mechanical Phenomena in Crystals. Dover, New York.

Catalan, G., Lubk, A., Vlooswijk, A.H.G., Snoeck, E., Magen, C., Janssens, A., Rispens, G., Rijnders, G., Blank, D.H.A., Noheda, B., 2011. Flexoelectric rotation of polarization in ferroelectric thin films. Nat. Mater. 10, 963-967.

Cross, L.E., 2006. Flexoelectric effects: Charge separation in insulating solids subjected to elastic strain gradients. J. Mater. Sci. 41, 53-63.

Curie, J., Curie, P., 1880. Comptes rendus hebdomadaires des séances de l'Académie des sciences 91, 294-295.

Darrall, B.T., Dargush, G.F., Hadjesfandiari, A.R., 2014. Finite element Lagrange multiplier formulation for size-dependent skew-symmetric couple-stress planar elasticity. Acta Mech. 225, 195-212.

Davis, T.A., 2004. A column pre-ordering strategy for the unsymmetric-pattern multifrontal method. ACM Trans. Math. Software 30, 165-195.

Davis, T.A., Duff, I.S., 1997. An unsymmetric-pattern multifrontal method for sparse LU factorization. SIAM J. Matrix Anal. Appl. 18, 140-158.

Eliseev, E.A., Morozovska, A.N., Glinchuk, M.D., Blinc, R., 2009. Spontaneous flexoelectric/ flexomagnetic effect in nanoferroics. Phys. Rev. B 79, 165433.

Gaudenzi, P., Bathe, K.J., 1995. An iterative finite-element procedure for the analysis of piezoelectric continua. J. Intell. Mater. Sys. Struct. 6, 266-273.

Griffiths, D.J., 1989. Introduction to Electrodynamics. Prentice Hall, Englewood Cliffs, N.J.

Hadjesfandiari, A.R., 2013. Size-dependent piezoelectricity. Int. J. Solids Struct. 50, 2781-2791.

Hadjesfandiari, A.R., 2014. Size-dependent theories of piezoelectricity: Comparisons and further developments for centrosymmetric dielectrics. Nanotech. In review.

Hadjesfandiari, A.R., Dargush, G.F., 2011. Couple stress theory for solids. Int. J. Solids Struct. 48, 2496-2510.

Hadjesfandiari, A.R., Dargush, G.F., 2013. Fundamental solutions for isotropic size-dependent couple stress elasticity. Int. J. Solids Struct. 50, 1253-1265.

Harden, J., Mbanga, B., Eber, N., Fodor-Csorba, K., Sprunt, S., Gleeson, J.T., Jakli, A., 2006. Giant flexoelectricity of bent-core nematic liquid crystals. Phys. Rev. Lett. 97, 157802.

Hwang, W.S., Park, H.C., Ha, S.K., 1993. Finite element modeling of piezoelectric sensors and actuators. AIAA J. 31, 930-937.

Jaffe, B., Cook, W. R., Jaffe, H. 1971. Piezoelectric ceramics. Academic Press, New York, N.Y.

Kogan, S.M., 1964. Piezoelectric effect during inhomogeneous deformation and acoustic scattering of carriers in crystals. Sov. Phys. Solid State 5, 2069-2070.

Koiter, W.T., 1964. Couple stresses in the theory of elasticity, I and II. Proc. Kon. Neder. Akad. Weten. B 67, 17-44.

Li, A., Zhou, S., Zhou, S., Wang, B., 2014. Size-dependent analysis of a three-layer microbeam including electromechanical coupling. Compos. Struct. 116, 120-127.

Ma, W., Cross, L.E. 2006. Flexoelectricity of barium titanate. Appl. Phys. Lett. 88, 232902.

Majdoub, M.S., Sharma, P., Cagin, T., 2008. Enhanced size-dependent piezoelectricity and elasticity in nanostructures due to the flexoelectric effect. Phys. Rev. B 77, 125424.

Maranganti, R., Sharma, P., 2009. Atomistic determination of flexoelectric properties of crystalline dielectrics. Phys. Rev. B 80, 054109.

Maranganti, R., Sharma, N.D., Sharma, P., 2006. Electromechanical coupling in nonpiezoelectric materials due to nanoscale nonlocal size effects: Green's function solutions and embedded inclusions. Phys. Rev. B 74, 014110.

MATLAB (2014). Release 2014a, The MathWorks, Inc., Natick, MA.

Meyer, R.B., 1969. Piezoelectric effects in liquid crystals. Phys. Rev. Lett. 22, 918-921.

Mindlin, R.D., Tiersten, H.F., 1962. Effects of couple-stresses in linear elasticity. Arch. Ration. Mech. Anal. 11, 415-448.

Mishima, T., Fujioka, H., Nagakari, S., Kamigaki, K., Nambu, S., 1997. Lattice image observations of nanoscale ordered regions in Pb (Mg1/3Nb2/3)O-3. Jpn. J. App. Phys. 36, 6141-6144.

Resta, R., 2010. Towards a bulk theory of flexoelectricity. Phys. Rev. Lett. 105, 127601.

Sharma, N.D., Maranganti, R., Sharma, P., 2007. On the possibility of piezoelectric nanocomposites without using piezoelectric materials. J. Mech. Phys. Solids 55, 2328-2350.

Shvartsman, V.V., Emelyanov, A.Y., Kholkin, A.L., Safari, A., 2002. Local hysteresis and grain size effects in Pb(Mg1/3Nb2/3)O-SbTiO3. Appl. Phys. Lett. 81, 117-119.

Tagantsev, A.K., 1986. Piezoelectricity and flexoelectricity in crystalline dielectrics. Phys. Rev. B 34, 5883-5889.

Toupin, R.A., 1962. Elastic materials with couple-stresses. Arch. Ration. Mech. Anal. 11, 385-414.

Voigt, W., 1910. Lehrbuch der Kristallphysik. BG Teubner, Berlin.

Wang, G.F., Yu, S.W., Feng, X.Q., 2004. A piezoelectric constitutive theory with rotation gradient effects. Eur. J. Mech. A/Solids 23, 455-466.

Yudin, P.V., Tagantsev, A.K., 2013. Fundamentals of flexoelectricity in solids. Nanotechnology 24, 432001.

Zhu, W., Fu, J.Y., Li, N., Cross, L.E., 2006. Piezoelectric composite based on the enhanced flexoelectric effects. Appl. Phys. Lett. 89, 192904.

Zienkiewicz, O.C., Taylor, R.L., 2000. The Finite Element Method. Butterworth-Heinemann, Oxford.

Zubko, P., Catalan, G., Buckley, A., Welche, P.R.L., Scott, J.F., 2007. Strain-gradient-induced polarization in SrTiO3 single crystals. Phys. Rev. Lett. 99, 167601.

Zubko, P., Catalan, G., Tagantsev, A.K., 2013. Flexoelectric effect in solids. Ann. Rev. Mater. Res. 43, 387-421.